In vitro and *in vivo* two-photon luminescence imaging of single gold nanorods

Haifeng Wang*, Terry B. Huff†, Daniel A. Zweifel†, Wei He†, Philip S. Low†, Alexander Wei†‡, and Ji-Xin Cheng*†§

*Weldon School of Biomedical Engineering and †Department of Chemistry, Purdue University, West Lafayette, IN 47907

Edited by Y. Ron Shen, University of California, Berkeley, CA, and approved September 14, 2005 (received for review June 11, 2005)

Gold nanorods excited at 830 nm on a far-field laser-scanning microscope produced strong two-photon luminescence (TPL) intensities, with a $\cos^4$ dependence on the incident polarization. The TPL excitation spectrum can be superimposed onto the longitudinal plasmon band, indicating a plasmon-enhanced two-photon absorption cross section. The TPL signal from a single nanorod is 58 times that of the two-photon fluorescence signal from a single rhodamine molecule. The application of gold nanorods as TPL imaging agents is demonstrated by *in vivo* imaging of single nanorods flowing in mouse ear blood vessels.

in vivo imaging | plasmon resonance | multiphoton | nonlinear optics

Photoluminescence from noble metals was first reported in 1969 by Mooradian (1) and later observed as a broad background in surface-enhanced Raman scattering (2). Single-photon luminescence from metals has been described as a three-step process as follows: (*i*) excitation of electrons from the *d*- to the *sp*-band to generate electron–hole pairs, (*ii*) scattering of electrons and holes on the picosecond timescale with partial energy transfer to the phonon lattice, and (*iii*) electron–hole recombination resulting in photon emission (1). Two-photon luminescence (TPL) was characterized by Boyd *et al.* (3) and is considered to be produced by a similar mechanism as single-photon luminescence, but the relatively weak TPL signal can be amplified by several orders of magnitude when produced from roughened metal substrates. This amplification is due to a resonant coupling with localized surface plasmons, which are well known to enhance a variety of linear and nonlinear optical properties (4–9).

Metal nanoparticles are also capable of photoluminescence, which has been shown to correlate strongly with their well-defined plasmon resonances (10–16). For example, Mohamed *et al.* (11) have observed that the quantum efficiency of single-photon luminescence from gold nanorods is enhanced by a factor of >1 million under plasmon-resonant conditions. Plasmon-resonant TPL is attractive for nonlinear optical imaging of biological samples with 3D spatial resolution (17). Gold nanorods are particularly appealing as TPL substrates because their longitudinal plasmon modes are resonant at near-infrared, where the absorption of water and biological molecules are minimized. Moreover, nanorods have larger local field enhancement factors than nanoparticles due to reduced plasmon damping (18). A scanning near-field optical microscopy study of TPL from single nanorods (diameter ≈ 40 nm) has recently been reported by Imura *et al.* (16), who observed that the luminescence is greatest at their tips. However, further characterization of TPL from single gold nanorods is needed: the polarization dependence of TPL excitation and emission from nanorods has yet to be defined, as well as the relationship between TPL enhancement and the longitudinal and transverse plasmon modes. These studies can provide a deeper understanding of single-particle TPL and its potential application in nonlinear optical imaging.

In this work, we use a two-photon excitation laser-scanning microscope to study plasmon-resonant TPL from single gold nanorods. The emission spectrum of the TPL is characterized as a function of excitation wavelength and polarization. We find that the TPL signal from a single nanorod is essentially depolarized yet has a $\cos^4$ dependence on the excitation polarization and is nearly 60 times brighter than the two-photon fluorescence (TPF) from a single rhodamine molecule. These features render gold nanorods as a unique imaging agent for multiphoton microscopy, which we demonstrate *in vivo* by using TPL to monitor the flow of single nanorods through mouse ear blood vessels.

Materials and Methods

Gold nanorods were prepared by seeded growth in micellar solutions of cetyltrimethylammonium bromide (0.2 M) with $AgNO_3$ as an additive (19, 20), followed by treatment with Na_2S 15 min after injection of the seed solution to arrest further growth and subsequent blueshifting of their optical resonances (21). The sulfide-treated nanorods were isolated by centrifugation (1 min, 12,500 × *g*) and redispersed in deionized water. Transmission electron microscopy (TEM) revealed dumbbell-shaped nanorods with an average aspect ratio of 3 (Fig. 1*a*). An extinction spectrum of the nanorod dispersion indicated a longitudinal plasmon mode centered at 820 nm and a weak transverse plasmon mode at 525 nm.

A femtosecond Ti:Sapphire laser (Mira 900, Coherent, Santa Clara, CA) was used to generate the TPL from gold nanorods. The output laser pulse has a duration of 200 fs and a repetition rate of 77 MHz. The laser beam was directed into a scanning confocal microscope (FV300/IX70, Olympus, Melville, NY) by using a ×60 water-immersion objective to focus the laser beam (focal width ≈230 nm) onto the nanorods, which were dispersed on a clean coverslip. The excitation field polarization was controlled by a halfwave plate in the incident beam. The TPL from nanorods was collected through the same objective, separated from the excitation laser by a dichroic mirror, and detected with a photomultiplier tube (PMT) (H7422-40, Hamamatsu, Bridgewater, NJ) placed in the back port of the microscope. A bandpass filter with a transmission window from 400 to 670 nm (35-5461, Ealing Catalog, Rocklin, CA) was placed before the PMT to minimize the count of adventitious photons from the excitation source. The TPL also was measured with a spectrometer (Shamrock 303i, Andor Technology, Belfast, Ireland), and emission polarization was gauged by rotating a polarizer plate before the PMT.

Light-correlation spectroscopy (22) was used to analyze the freely diffusing nanorods. The original nanorod solution was diluted 10 times and then briefly sonicated. Time-resolved TPL traces were recorded by using the point-scanning mode on

Conflict of interest statement: No conflicts declared.

This paper was submitted directly (Track II) to the PNAS office.

Abbreviations: TPL, two-photon luminescence; TPF, two-photon fluorescence.

‡To whom correspondence may be addressed at: Department of Chemistry, 560 Oval Drive, West Lafayette, IN 47907. E-mail: alexwei@purdue.edu.

§To whom correspondence may be addressed at: Weldon School of Biomedical Engineering, Purdue University, 500 Central Drive, West Lafayette, IN 47907. E-mail: jcheng@purdue.edu.

www.pnas.org/cgi/doi/10.1073/pnas.0504892102

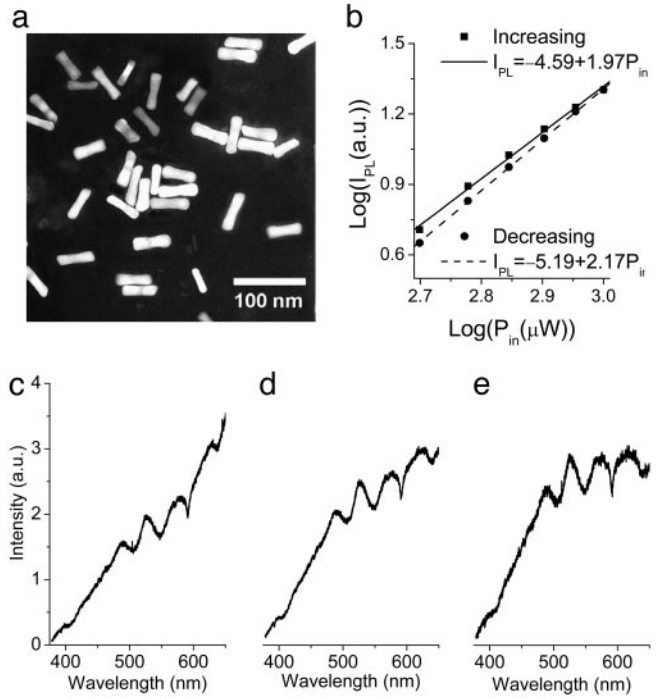

Fig. 1. Properties of TPL from Au nanorods. (*a*) TEM image (Philips CM-10, 80 kV) of Au nanorods, treated with 0.5 mM Na_2S to arrest further growth. Nanorod suspensions were cast onto carbon-coated Cu grids, then blotted after 30 sec and dried in air. Average nanorod length and midsection was determined to be 48.6 ± 6.7 and 15.8 ± 2.5 nm, respectively. (*b*) Dependence of the luminescence intensity on the excitation power. The data were obtained by increasing the excitation pulse energy from 1 to 2 pJ, then decreasing the power accordingly. The slope values are close to 2.0, indicative of TPL. Signal intensities were integrated over an area of 250 × 250 μm. (*c–e*) Photoluminescence spectra from a solution of gold nanorods at excitation wavelengths of 730 (*c*), 780 (*d*), and 830 (*e*) nm, respectively. The spectrum is cut off at 670 nm by the bandpass filter. a.u., arbitrary units.

the FV300 confocal microscope. The TPL autocorrelation curves were calculated and fitted according to a 3D diffusion model (23).

Balb/C female mice[¶] were used for *in vivo* imaging of gold nanorods. A 6- to 8-week-old mouse was anesthetized by intraperitoneal injection of avertin (500 mg/kg) before introducing 200 μl of nanorod solution (1:4 diluted with PBS buffer) into the animal's vasculature via tail vein injection. The mouse was placed on a Petri dish with one ear attached to the coverslip bottom, by using glycerol as an interstitial medium to reduce optical interference. A ×40 water-immersion objective with a working distance of 3.3 mm was used to focus the femtosecond laser beam onto the ear lobe. The laser power at the sample was ≈18 mW. Transmission and TPL imaging were carried out simultaneously.

Results and Discussion

Incident Pulse Energy Dependence. The nonlinear nature of the TPL signal was confirmed by measuring the dependence of the luminescence intensity as a function of excitation power. Signal intensities were collected for increasing incident pulse energies from 1 to 2 pJ, then again for decreasing pulse energies from 2 to 1 pJ (see Fig. 1*b*). For a 1-pJ energy pulse, we estimate a single nanorod to receive ≈15 fJ, which is below the accepted damage threshold of 60 fJ (24). A quadratic dependence of the signal intensity on the input power was observed, with slope values of 1.97 for the increasing power curve and 2.17 for the decreasing power curve. This small discrepancy could be due to the melting of a small portion of nanorods at high power.

[¶]The animal study protocol has been approved by Purdue University Animal Care and Use Committee (no. 96-069-02).

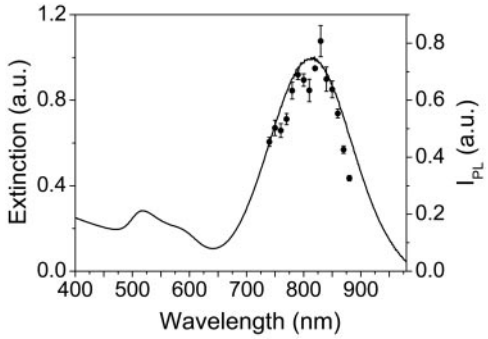

Fig. 2. Linear absorption of the gold nanorods (solid line) compared with the TPL excitation spectrum (solid circles with error bars). The peak at 820 nm corresponds to the longitudinal plasmon mode. The same power (0.17 mW) was used for all excitation wavelengths.

Emission Spectrum. TPL spectra were obtained by using a solution of gold nanorods at different excitation wavelengths (see Fig. 1 *c–e*). The suspension of cetyltrimethylammonium bromide-coated nanorods was immersed briefly in an ultrasonic bath to minimize aggregation effects. The broadband emission spectrum in the 400- to 650-nm region includes the 6–5L transition (electron–hole recombination) and 6–5X transition, which occurs for bulk gold at 518 and 654 nm, respectively (3). The peak positions in the TPL spectra are independent of the excitation energy. Irradiation of the nanorods at the same excitation power, but with the laser running in cw mode, reduces the signal intensity to background noise level, thus confirming that the emission spectra are due to TPL.

Excitation Profile. To determine the relationship between the observed TPL and the longitudinal plasmon mode of the gold nanorods, we profiled the dependence of TPL intensity on the excitation wavelength against the extinction spectrum, also measured from solution (see Fig. 2). We find that the excitation spectrum (solid circles) overlaps well with the longitudinal plasmon band, indicating that the TPL intensity is governed by the local field enhancement from the plasmon resonance. This result is consistent with the calculation by Bouhelier *et al.* (13), who showed that the field enhancement maximum coincides with the plasmon resonance of a gold nanoparticle dimer. We note that the excitation spectrum near plasmon resonance has a narrower bandwidth than the single-photon absorbance peak because of the nonlinear character of TPL, but both are broader than the emission spectrum measured for an individual nanorod (18). The broadening is likely due to the distribution of the nanorods' aspect ratios, which range from 2.3 to 4.2.

Dependence on Excitation Polarization. The TPL intensity of the nanorods was examined as a function of polarization angle of the incident beam (see Fig. 3; see also Movie 1, which is published as supporting information on the PNAS web site). TPL enhancement should be maximized when the incident field is aligned with the dipolar plasmon resonance with its polarization along the long axis of the nanorod (25, 26). TPL images of nanorods with horizontally and vertically polarized excitation (Fig. 3 *a* and *b*, respectively) display many spots within the same intensity range, indicating contributions from single nanorods (e.g., spots 1 and 2); brighter sites are assumed to be clusters of nanorods (e.g.,

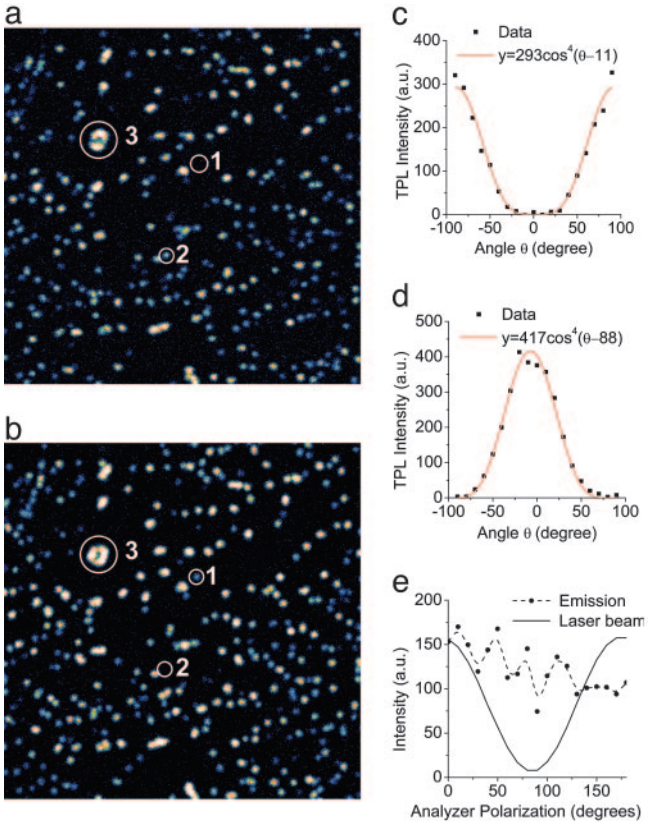

Fig. 3. Nanorod TPL intensity as a function of excitation polarization. (*a* and *b*) Pseudocolor images with horizontal (*a*, $\theta = 0°$) and vertical (*b*, $\theta = 90°$) excitation polarizations, respectively. Nanorods were dispersed onto a glass coverslip; image size is 25 × 25 μm. Single nanorods could be identified by their similar range of intensities during polarization; brighter spots are considered to be produced by clusters of nanorods. (*c*) Polarization dependence of the TPL intensity (solid dots) for a single nanorod (spot 1). The excitation polarization was rotated clockwise from −90° to +90° in 10° increments. The polarization-dependent TPL fits a $\cos^4$ function, offset by 88.2° (red curve). (*d*) Polarization dependence of TPL intensity (solid dots) for a second single nanorod (spot 2). The polarization-dependent TPL again fits a $\cos^4$ function, offset by 6.8° (red curve). (*e*) The emission polarization of TPL (solid dots) from the same nanorod (spot 2) measured by rotating a polarizer before the detector. In comparison, the reflected excitation laser beam (solid curve) is linearly polarized at the detector site.

spot 3). All emissions were observed to be sensitive to the incident polarization: for example, polarization-dependent excitation was readily observed for the ring-like cluster in spot 3, with different parts being excited by horizontal or perpendicular polarization, respectively.

To quantify the relationship between nanorod orientation and incident polarization, we measured the TPL intensity from different sites as a function of the incident polarization angle θ, assuming 0° for horizontal polarization. Two typical results are shown in Fig. 3 *c* and *d*; in both cases, the data can be fitted to a $\cos^4$ function. These results also indicate an orientational dependency on a single dipole, implying that the contribution from the transverse mode to TPL is negligible. Because the excitation polarization is linear and precisely defined, the relative orientation of the nanorods can be accurately determined by using a least-squares fit. According to the derivations of Boyd *et al.* (25) for polarization-dependent field effects from metal substrates with anisotropic surface roughness, the local field enhancement $|E/E_0|^2$ is proportional to $[E_{in}\cos(\theta + \alpha)]^2$ or $I_{in}\cos^2(\theta + \alpha)$. The corresponding TPL intensity is thus proportional to $I_{in}^2\cos^4(\theta + \alpha)$, where $\theta + \alpha$ is the angle between the polarized incident field E_{in} and the nanorod long axis and I_{in} is the incident field intensity. The TPL from a single nanorod has the same polarization dependence as the TPF from a single fluorescent molecule, in accord with the dipolar nature of the nanorods' plasmon resonance.

Emission Polarization. The TPL from gold nanorods was determined to be essentially depolarized (see Fig. 3*e*; see also Movie 2, which is published as supporting information on the PNAS web site). The reflected excitation beam also was measured at the detector position as a control and was observed to be linearly polarized. In this regard, the incoherent TPL has more in common with plasmon-enhanced second-harmonic generation signals, which also have been shown to be strongly depolarized (27), than with plasmon-resonant scattering processes, which retain the polarization of the incident beam (18, 28). Furthermore, whereas the TPL excitation correlates strongly with longitudinal plasmon resonance, the TPL emission spectrum appears to be very broad and is likely to be produced directly by electron–hole recombination rather than through intermediate particle plasmons in the single-photon luminescence of gold nanoparticles as recently proposed by Dulkeith *et al.* (29). Therefore, the plasmon-enhanced TPL from nanorods is essentially due to a greater two-photon absorption cross section.

Brightness Characterization. The TPL intensity from single nanorods was compared with the TPF from single rhodamine molecules. A drop of dilute aqueous solution of rhodamine 6G (1 pM) was dried on a glass coverslip, then irradiated at 5 mW at 830 nm under the same conditions used for collecting TPL signal from nanorods. The single-molecule TPF signals also could be verified by the $\cos^4$ dependence of their excitation polarization. In this manner, we determined that the TPL intensity from a typical gold nanorod in our sample is ≈58 times brighter than the TPF from a single rhodamine molecule under identical excitation conditions.

This comparison enables us to quantify the TPL brightness, which can be described in terms of an action cross section $\varphi_{2p} = \sigma_{2p} \times \eta$, where σ_{2p} is the two-photon absorption cross section and η is the quantum efficiency. Previous measurements of φ_{2p} for rhodamine 6G yielded a value of 40 Göppert-Mayer units (GM; 1 GM = 10^{-50} cm^4·s/photon) at 830 nm (30), so the corresponding φ_{2p} for our nanorods is 2,320 GM. This value is within the range of φ_{2p} values determined for quantum dots (2,000–47,000 GM) (31). It is worth noting that in addition to their enhanced TPL, the gold nanorods can provide orientational information as recently demonstrated by Sönnichsen and Alivisatos (28). The gold nanorods are also essentially inert to photobleaching, a quality whose practical consequences are widely appreciated in biophotonic applications (17, 28).

TPL Autocorrelation Measurements. Correlation spectroscopy (22) was used to determine the diffusion modes and the density of nanorods in the solution. A typical TPL fluctuation curve is shown in Fig. 4 *Inset*, with intermittent spikes in intensity produced by the diffusion of single nanorods into the focal volume. Consistent results were obtained from 10 independent traces. The focus profile was assumed to be Gaussian with a lateral e^{-2} width of $r_0 = 0.34$ μm and an axial width of $z_0 = 1.1$ μm. The autocorrelation curve was calculated from the fluctuation trace and fitted according to a 3D diffusion model for two-photon excitation fluorescence correlation spectroscopy (23)

$$G(\tau) = \frac{1}{\langle N \rangle}\left(1 + \frac{\tau}{\tau_D}\right)^{-1}\left(1 + \frac{r_0^2\tau}{z_0^2\tau_D}\right)^{-1/2}.$$

The autocorrelation curve could be fitted by using a single time constant, indicating isotropic diffusion; a separate component

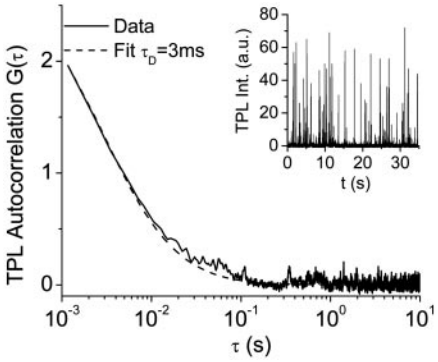

Fig. 4. TPL autocorrelation curve (solid) and fluctuation trace (*Inset*) measured from a dilute nanorod solution. The fit curve (dashed) was performed by using a single time constant.

for nanorod rotational motion could not be distinguished. The diffusion time τ_D and the average nanorod number $\langle N \rangle$ were determined to be 3.0 ms and 0.5, respectively. With the excitation volume calculated as $(\pi/2)^{3/2} r_0^2 z_0$ (23), the molar concentration of the undiluted nanorod solution was determined to be 34 nM. By comparing the diffusion constant $D = r_0^2/(8\tau_D)$ to the Stokes–Einstein relation $D = kT/(3\pi\eta d)$ where the viscosity of water $\eta = 9.8 \times 10^{-4}$ N·s^{-1}·m^{-2}, we found the average hydrodynamic diameter of the diffusing particle to be 92 nm. This value is larger than the dimensions of the nanorods measured by TEM, possibly due to the contributions from the cetyltrimethylammonium bromide coating.

***In Vivo* Imaging.** The nanorods' plasmon resonance in the near IR region makes them ideal probes for TPL imaging of tissue samples, complementary to the use of semiconductor quantum dots (31). Whereas the linear plasmon-resonant scattering is essentially limited to 2D imaging, the TPL signal is resolved in the axial direction because of its nonlinear dependence on the excitation intensity. In our case, the full width at half maximum of the lateral and axial TPL intensity profile from a single nanorod were measured to be ≈0.3 and 1.0 μm, respectively. The intrinsic 3D spatial resolution of TPL is useful for monitoring biological processes in real time, which we demonstrate below by *in vivo* imaging of single nanorods flowing through the blood vessels in a mouse earlobe.

Two earlobe vessels were selected by using transmission illumination and monitored for nearly 10 min (see Fig. 5*a*; see also Movie 3, which is published as supporting information on the PNAS web site). The quantity of nanorods injected was estimated to be 1.7 pmol based on the molar concentration derived from the autocorrelation measurement. We note that this quantity is much less than the amount of quantum dots used (32 pmol) in a recent work involving a similar mouse model (31). Fig. 5 *b* and *c* are still images of nanorods (stack of 300 frames and single frame, respectively) 5 min after injection into the mouse tail vein, with the nanorods appearing as isolated red dots. The uniform intensity of the TPL signals in the single-frame image indicates that most of the dots are produced by single nanorods (see Fig. 5*d* for intensity profile). The TPL intensity from individual nanorods is approximately three times that of the autofluorescence from the blood and surrounding tissue. Because the flowing nanorods were exposed to laser irradiation for a very short time, the possibility of their thermal degradation during the experiment was very remote. After 30 min, we could no longer detect TPL signals from nanorods in the blood vessels. This rapid clearance time suggests that gold nanorods will provide excellent TPL contrast when functionalized for cell-specific labeling.

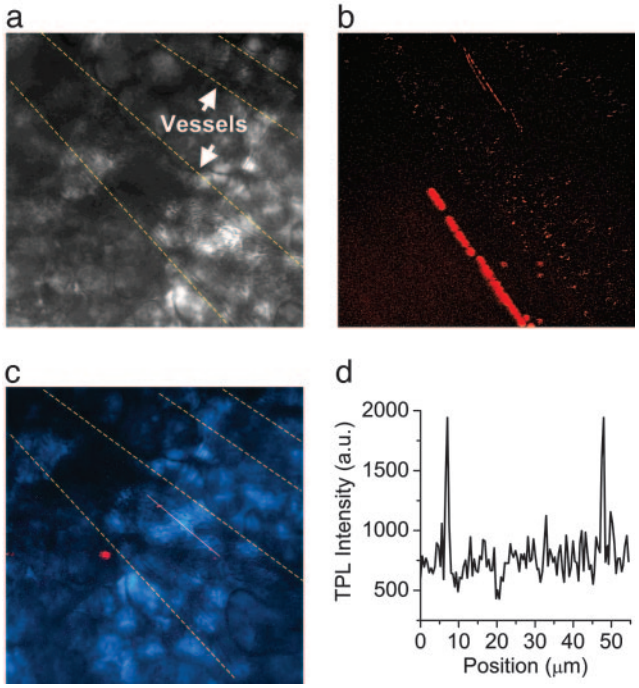

Fig. 5. *In vivo* imaging of single gold nanorods in mouse ear blood vessels. (*a*) Transmission image with the two blood vessels indicated. Dotted contour lines are provided to guide the eye. (*b*) TPL image of gold nanorods (red dots) flowing through the blood vessels. Image was compiled as a stack of 300 frames collected continuously at a rate of 1.12 sec per frame. The excitation power at the sample was 18 mW with an excitation wavelength of 830 nm; image size is 175 × 175 μm. The bright signal beneath the lower blood vessel is the autofluorescence from a hair root. The streaking is due to sample drift during imaging. (*c*) Overlay of the transmission image (light blue) and a single-frame TPL image. Two single nanorods (red spots) are superimposed by a linescan (white). (*d*) TPL intensity profile from the linescan in *c*. The background (≈750 a.u.) is due to autofluorescence from the blood vessel and the surrounding tissue. The similar intensities of the red spots indicate the detection of single nanorods.

Conclusions

The TPL intensities from single gold nanorods is many times brighter than the TPF from single dye molecules and exhibit a cos^4 dependence on excitation polarization, which may be useful in providing additional orientation information. The TPL excitation spectrum overlaps with the longitudinal plasmon band, indicating that the two-photon absorption cross section is enhanced by plasmon resonance. These features, coupled with the intrinsic 3D spatial resolution of nonlinear optical processes, open up exciting possibilities for using gold nanorods as biological imaging agents.

We thank Hongtao Chen for his assistance with several optical experiments. This work was supported by National Institutes of Health Grant EB-001777-01, National Science Foundation Grants CHE-0243496 and ECS-0210445, and startup funds from Purdue University.

1. Mooradian, A. (1969) *Phys. Rev. Lett.* **22,** 185–187.
2. Heritage, P., Bergman, J. G., Pinczuk, A. & Worlock, J. M. (1979) *Chem. Phys. Lett.* **67,** 229–232.
3. Boyd, G. T., Yu, Z. H. & Shen, Y. R. (1986) *Phys. Rev. B Condens. Matter* **33,** 7923–7936.
4. Kreibig, U. & Vollmer, M. (1995) *Optical Properties of Metal Clusters* (Springer, Berlin).
5. Wei, A. (2004) in *Nanoparticles: Scaffolds and Building Blocks*, ed. Rotello, V. M. (Kluwer Academic, New York), pp. 173–200.
6. Moskovits, M. (1985) *Rev. Mod. Phys.* **57,** 783–828.
7. Chen, C. K., de Castro, A. R. B. & Shen, Y. R. (1981) *Phys. Rev. Lett.* **46,** 145–148.
8. Sánchez, E. J., Novotny, L. & Xie, X. S. (1999) *Phys. Rev. Lett.* **82,** 4014–4017.
9. Dickson, R. M. & Lyon, L. A. (2000) *J. Phys. Chem. B* **104,** 6095–6098.

10. Wilcoxon, J. P., Martin, J. E., Parsapour, F., Wiedenman, B. & Kelley, D. F. (1998) *J. Chem. Phys.* **108,** 9137–9143.
11. Mohamed, M. B., Volkov, V., Link, S. & El-Sayed, M. A. (2000) *Chem. Phys. Lett.* **317,** 517–523.
12. Peyser, L. A., Lee, T. H. & Dickson, R. M. (2002) *J. Phys. Chem. B* **106,** 7725–7728.
13. Bouhelier, A., Beversluis, M. R. & Novotny, L. (2003) *Appl. Phys. Lett.* **83,** 5041–5043.
14. Beversluis, M. B., Bouhelier, A. & Novotny, L. (2003) *Phys. Rev. B Condens. Matter Mater. Phys.* **68,** 115433.
15. Drachev, V. P., Khaliullin, E. N., Kim, W., Alzoubi, F., Rautian, S. G., Safonov, V. P., Armstrong, R. L. & Shalaev, V. M. (2004) *Phys. Rev. B Condens. Matter Mater. Phys.* **69,** 035318.
16. Imura, K., Nagahara, T. & Okamoto, H. (2004) *J. Am. Chem. Soc.* **126,** 12730–12731.
17. Yelin, D., Oron, D., Thiberge, S., Moses, E. & Silberberg, Y. (2003) *Opt. Express.* **11,** 1385–1391.
18. Sönnichsen, C., Franzl, T., Wilk, T., von Plessen, G., Feldmann, J., Wilson, O. & Mulvaney, P. (2002) *Phys. Rev. Lett.* **88,** 077402.
19. Nikoobakht, B. & El-Sayed, M. A. (2003) *Chem. Mater.* **15,** 1957–1962.
20. Jana, N. R., Gearheart, L. & Murphy, C. J. (2001) *Adv. Mater.* **13,** 1389–1393.
21. Zweifel, D. A. & Wei, A. (2005) *Chem. Mater.* **17,** 4256–4261.
22. Elson, E. L., Magde, D. & Webb, W. W. (1974) *Biopolymers* **13,** 29–61.
23. Berland, K. M., So, P. T. C. & Gratton, E. (1995) *Biophys. J.* **68,** 694–701.
24. El-Sayed, M. A. (2001) *Acc. Chem. Res.* **34,** 257–264.
25. Boyd, G. T., Rasing, T., Leite, J. R. R. & Shen, Y. R. (1984) *Phys. Rev. B Condens. Matter* **30,** 519–526.
26. Novotny, L., Bian, X. R. & Xie, X. S. (1997) *Phys. Rev. Lett.* **79,** 645–648.
27. Anceau, C., Brasselet, S., Zyss, J. & Gadenne, P. (2003) *Opt. Lett.* **28,** 713–715.
28. Sönnichsen, C. & Alivisatos, A. P. (2005) *Nano. Lett.* **5,** 301–304.
29. Dulkeith, E., Niedereichholz, T., Klar, T. A., Feldmann, J., von Plessen, G., Gittins, D. I., Mayya, K. S. & Caruso, F. (2004) *Phys. Rev. B Condens. Matter Mater. Phys.* **70,** 205424.
30. Albota, M. A., Xu, C. & Webb, W. W. (1998) *Appl. Opt.* **37,** 7352–7356.
31. Larson, D. R., Zipfel, W. R., Williams, R. M., Clark, S. W., Bruchez, M. P., Wise, F. W. & Webb, W. W. (2003) *Science* **300,** 1434–1436.